EUROPEAN ORGANIZATION FOR NUCLEAR RESEARCH

CERN–EP/99-61
April 16, 1999

Spin Asymmetries A_1 of the Proton and the Deuteron in the Low x and Low Q^2 Region from Polarized High Energy Muon Scattering

The Spin Muon Collaboration (SMC)

Abstract

We present the results of the spin asymmetries A_1 of the proton and the deuteron in the kinematic region extending down to $x = 6 \cdot 10^{-5}$ and $Q^2 = 0.01$ GeV^2. The data were taken with a dedicated low x trigger, which required hadron detection in addition to the scattered muon, so as to reduce the background at low x. The results complement our previous measurements and the two sets are consistent in the overlap region. No significant spin effects are found in the newly explored region.

To be Submitted to Physical Review D

B. Adeva[20], E. Arik[2], A. Arvidson[23,w], B. Badełek[23,25], G. Baum[1], P. Berglund[8], L. Betev[13,p], N. de Botton[19], F. Bradamante[22], A. Bravar[11], S. Bültmann[1,b], E. Burtin[19], D. Crabb[24], J. Cranshaw[18,c], T. Çuhadar[2,15], S. Dalla Torre[22], R. van Dantzig[15], B. Derro[4], A. Deshpande[26], S. Dhawan[26], C. Dulya[4,d], S. Eichblatt[18,e], D. Fasching[17,f], F. Feinstein[19], C. Fernandez[20,9], B. Frois[19], A. Gallas[20], J.A. Garzon[20,9], H. Gilly[6], M. Giorgi[22], E. von Goeler[16], S. Goertz[3], G. Gracia[20,g], N. de Groot[15,h], M. Grosse Perdekamp[26,i], K. Haft[13], D. von Harrach[11], T. Hasegawa[14,j], P. Hautle[5,k], N. Hayashi[14,l], C.A. Heusch[5,m], N. Horikawa[14], V.W. Hughes[26], G. Igo[4], S. Ishimoto[14,n], T. Iwata[14], E.M. Kabuß[11], A. Karev[10], H.J. Kessler[6,o], T.J. Ketel[15], J. Kiryluk[23,25], Yu. Kisselev[10], D. Krämer[1], W. Kröger[5,m], K. Kurek[25], J. Kyynäräinen[1,8], M. Lamanna[22,a], U. Landgraf[6], J.M. Le Goff[19], F. Lehar[19], A. de Lesquen[19], J. Lichtenstadt[21], M. Litmaath[15,a], A. Magnon[19], G.K. Mallot[11,a], F. Marie[19], A. Martin[22], J. Martino[19], T. Matsuda[14,j], B. Mayes[9], J.S. McCarthy[24], K. Medved[10], W. Meyer[3], G. van Middelkoop[15], D. Miller[17], Y. Miyachi[14], K. Mori[14], J. Moromisato[16], J. Nassalski[25], T.O. Niinikoski[5], J.E.J. Oberski[15], A. Ogawa[14], C. Ozben[2], H. Pereira[19], F. Perrot-Kunne[19], D. Peshekhonov[10,c], R. Piegaia[26,q], L. Pinsky[9], S. Platchkov[19], M. Plo[20], D. Pose[10], H. Postma[15], J. Pretz[11,z], R. Puntaferro[22], G. Rädel[5], G. Reicherz[3], J. Roberts[r], M. Rodriguez[23,q], E. Rondio[25], I. Sabo[21], J. Saborido[20], A. Sandacz[25], I. Savin[10], P. Schiavon[22], E.P. Sichtermann[15], F. Simeoni[22], G.I. Smirnov[10], A. Staude[13], A. Steinmetz[11,z], U. Stiegler[5], H. Stuhrmann[7], F. Tessarotto[22], D. Thers[19], W. Tłaczała[25,s], A. Tripet[1], G. Unel[2], M. Velasco[17,a], J. Vogt[13], R. Voss[5], C. Whitten[4], R. Willumeit[7], R. Windmolders[12], W. Wiślicki[25], A. Witzmann[6,t], A.M. Zanetti[22], K. Zaremba[25,s], J. Zhao[7,u]

[1] University of Bielefeld, Physics Department, 33501 Bielefeld, Germany[aaa]
[2] Bogaziçi University and Istanbul Technical University, Istanbul, Turkey[bbb]
[3] University of Bochum, Physics Department, 44780 Bochum, Germany[aaa]
[4] University of California, Department of Physics, Los Angeles, 90024 CA, USA[ccc]
[5] CERN, 1211 Geneva 23, Switzerland
[6] University of Freiburg, Physics Department, 79104 Freiburg, Germany[aaa]
[7] GKSS, 21494 Geesthacht, Germany[aaa]
[8] Helsinki University of Technology, Low Temperature Laboratory and Institute of Particle Physics Technology, Espoo, Finland
[9] University of Houston, Department of Physics, and Institute for Beam Particle Dynamics, Houston, 77204 TX, USA[ccc,ddd]
[10] JINR, Dubna, RU-141980 Dubna, Russia
[11] University of Mainz, Institute for Nuclear Physics, 55099 Mainz, Germany[aaa]
[12] University of Mons, Faculty of Science, 7000 Mons, Belgium
[13] University of Munich, Physics Department, 80799 Munich, Germany[aaa]
[14] Nagoya University, CIRSE and Department of Physics, Furo-Cho, Chikusa-Ku, 464 Nagoya, Japan[eee]
[15] NIKHEF, Delft University of Technology, FOM and Free University, 1009 AJ Amsterdam, The Netherlands[fff]
[16] Northeastern University, Department of Physics, Boston, 02115 MA, USA[ddd]
[17] Northwestern University, Department of Physics, Evanston, 60208 IL, USA[ccc,ddd]
[18] Rice University, Bonner Laboratory, Houston, 77251-1892 TX, USA[ccc]
[19] C.E.A. Saclay, DAPNIA, 91191 Gif-sur-Yvette, France[ggg]
[20] University of Santiago, Department of Particle Physics, 15706 Santiago de Compostela, Spain[hhh]
[21] Tel Aviv University, School of Physics, 69978 Tel Aviv, Israel[iii]
[22] INFN Trieste and University of Trieste, Department of Physics, 34127 Trieste, Italy
[23] Uppsala University, Department of Radiation Sciences, 75121 Uppsala, Sweden
[24] University of Virginia, Department of Physics, Charlottesville, 22901 VA, USA[ccc]
[25] Sołtan Institute for Nuclear Studies and Warsaw University, 00681 Warsaw, Poland[jjj]
[26] Yale University, Department of Physics, New Haven, 06511 CT, USA[ccc]
[a] Now at CERN, 1211 Geneva 23, Switzerland
[b] Now at University of Virginia, Department of Physics, Charlottesville, 22901 VA, USA[ccc]
[c] Now at Texas Technical University, Lubbock TX 79409-1051, USA
[d] Now at CIEMAT, Avda Complutense 22, 28040, Madrid, Spain
[e] Now at Fermi National Accelerator Laboratory, Batavia, 60510 Illinois, USA
[f] Now at University of Wisconsin, USA
[g] Now at NIKHEF, 1009 AJ Amsterdam, The Netherlands
[h] Now at Bristol University, Bristol, UK
[i] Now at Brookhaven National Laboratory,Upton, 11973 NY, USA
[j] Permanent address: Miyazaki University, Faculty of Engineering, 889-21 Miyazaki-Shi, Japan
[k] Permanent address: Paul Scherrer Institut, 5232 Villigen, Switzerland
[l] Permanent address: The Institute of Physical and Chemical Research (RIKEN), wako 351-01, Japan
[m] Permanent address: University of California, Institute of Particle Physics, Santa Cruz, 95064 CA, USA
[n] Permanent address: KEK, Tsukuba-Shi, 305 Ibaraki-Ken, Japan
[o] Now at SBC Warburg Dillon Read, CH-4002 Basel, Switzerland
[p] Now with University of California, Department of Physics, Los Angeles, 90024 CA, USA, permanent

1 Introduction

Polarized deep inelastic lepton-nucleon scattering is an important tool to study the spin structure of the nucleon. Measurements with polarized proton, deuteron and helium-3 targets have determined the spin dependent structure functions of the nucleon in a wide kinematic range. In this paper we present results for the virtual photon-proton and virtual photon-deuteron cross section asymmetries $A_1^{\rm p}$ and $A_1^{\rm d}$ obtained from inelastic muon–proton and muon–deuteron interactions at 190 GeV, at very low x and Q^2, extending our measurements down to $x = 6 \cdot 10^{-5}$. The data were collected with a "low x trigger" in which both a minimal energy deposit in the hadronic part of the calorimeter and the detection of a scattered muon were demanded. The hadron requirement reduces the background at low x, which is dominated by the contamination from muon scattering off atomic electrons at $x_{\mu {\rm e}} = m_{\rm e}/M_{\rm p}$ and by the radiative events.

Physics of high parton densities, i.e. at low values of x, is being studied intensively [1]. The measurements at HERA show [2] that the rise of the spin independent structure function F_2 with decreasing x is present even at the smallest values of Q^2, $Q^2 \sim 0.1$ GeV^2. For $Q^2 \gtrsim 1$ GeV^2, that rise can be described by the standard DGLAP QCD evolution. In the non-perturbative region ($Q^2 \lesssim 1$ GeV^2) several approaches have been proposed [1, 3] to join leptoproduction to photoproduction ($Q^2 = 0$ GeV^2).

Our new data cover the kinematic range $6 \cdot 10^{-5} < x < 0.15$ and $0.01 < Q^2 < 20$ GeV^2. They provide the first values of spin asymmetries below $x = 8 \cdot 10^{-4}$ and complement our recently published measurements [4] that were obtained in the region $8 \cdot 10^{-4} < x < 0.7$ and $0.2 < Q^2 < 100$ GeV^2.

2 Spin asymmetries

The virtual photon–proton (–deuteron) asymmetries $A_1^{\rm p,d}$ are defined as follows (see Ref. [5] for details):

$$A_1^{\rm p} = \frac{\sigma_{1/2} - \sigma_{3/2}}{\sigma_{1/2} + \sigma_{3/2}}, \qquad A_1^{\rm d} = \frac{\frac{1}{2}(\sigma_0 - \sigma_2)}{\frac{1}{3}(\sigma_0 + \sigma_1 + \sigma_2)}\ , \tag{1}$$

address at CERN, 1211 Geneva 23, Switzerland
[q] Permanent address: University of Buenos Aires, Physics Department, 1428 Buenos Aires, Argentina
[r] Permanent address: Rice University, Bonner Laboratory, Houston, TX 77251-1892, USA
[s] Permanent address: Warsaw University of Technology, 00-665 Warsaw, Poland
[t] Now at F.Hoffmann-La Roche Ltd., CH-4070 Basel, Switzerland
[u] Now at Oak Ridge National Laboratory, Oak Ridge, TN 37831-6393, USA
[w] Now at The Royal Library, 102 41 Stockholm, Sweden
[z] Now at Yale University, Department of Physics, New Haven, 06511 CT, USA
[aaa] Supported by the Bundesministerium für Bildung, Wissenschaft, Forschung und Technologie
[bbb] Partially supported by TUBITAK and the Centre for Turkish-Balkan Physics Research and Application (Bogaziçi University)
[ccc] Supported by the U.S. Department of Energy
[ddd] Supported by the U.S. National Science Foundation
[eee] Supported by Monbusho Grant-in-Aid for Scientific Research (International Scientific Research Program and Specially Promoted Research)
[fff] Supported by the National Science Foundation (NWO) of the Netherlands
[ggg] Supported by the Commissariat à l'Energie Atomique
[hhh] Supported by Comision Interministerial de Ciencia y Tecnologia
[iii] Supported by the Israel Science Foundation.
[jjj] Supported by KBN grant 2P03B 081 14 and 2P03B 132 14.

where σ_J is the absorption cross section of a transverse virtual photon by a proton (deuteron) with total spin projection J in the photon direction.

In the SMC experiment, cross section asymmetries for parallel and antiparallel configurations of longitudinal beam and target polarizations,

$$A_{\parallel}^{\mathrm{p,d}} = \frac{\sigma^{\uparrow\downarrow} - \sigma^{\uparrow\uparrow}}{\sigma^{\uparrow\downarrow} + \sigma^{\uparrow\uparrow}} \tag{2}$$

are determined. They are related to the spin asymmetries $A_1^{\mathrm{p,d}}$ and $A_2^{\mathrm{p,d}}$ in the following way [5]:

$$A_{\parallel}^{\mathrm{p,d}} = D(A_1^{\mathrm{p,d}} + \eta A_2^{\mathrm{p,d}}), \tag{3}$$

where D is the depolarization factor and η depends only on kinematic variables. In the kinematic region of our measurements η is small. This together with small values of the asymmetries $A_2^{\mathrm{p,d}}$ published in Ref. [6] allows us to neglect the second term in Eq. (3) and to account for it only in the systematic error estimate.

The definition of the depolarization factor D requires care. The present measurements extend to Q^2 values close to the kinematic limit $Q^2_{\mathrm{min}} \approx m_\mu^2 y^2/(1-y)$, where the scattering angle is zero ($y = (E - E')/E = \nu/E$). In this case one cannot neglect terms proportional to the muon mass squared in the expression for the cross section. One should also observe that in the relation (3) between $A_{\parallel}$, D and $A_{1,2}$, only $A_{\parallel}$ is an observable, directly connected with the cross section. Therefore the muon mass term can be included into the definition of either D or $A_{1,2}$, provided their product, $A_{\parallel}$, remains unchanged. We have chosen the former option in order to keep the definition of A_1 consistent with the one used in our previous publications, so that the depolarization factor D is defined as in Ref. [5]:

$$D = \frac{y(2-y)(1+\gamma^2 y/2)}{y^2(1+\gamma^2)(1-2m_\mu^2/Q^2)+2(1-y-\gamma^2 y^2/4)(1+R)}\ , \tag{4}$$

where $\gamma = \sqrt{Q^2}/\nu$ and $R = \sigma_{\mathrm{L}}/\sigma_{\mathrm{T}}$ is the ratio of the absorption cross sections for longitudinal and transverse virtual photons. With this definition, D becomes larger than unity at Q^2 close to Q^2_{min} and can no longer be interpreted as the fraction of the incident muon polarization carried by the virtual photon.

3 Experimental setup

The experiment was performed at the high energy muon beam [7] at CERN. The set-up consisted of (i) a large cryogenic target [8] with two cells containing target material polarized in opposite directions, (ii) an open magnetic spectrometer [5] for the measurement of scattered muons and produced hadrons, and (iii) a beam polarimeter [9]. The beam polarization was $P_\mu = -0.795 \pm 0.019$ for an average muon energy of 187.4 GeV. For the polarized proton and deuteron targets the materials used were ammonia (NH_3) and deuterated butanol (C_4D_9OD), respectively. The average proton and deuteron polarizations were 0.89 and 0.50 and were measured with relative accuracies of 2.7% and 2.1%, respectively. Events originating from both target cells were recorded simultaneously and the target spin orientations were reversed every five hours.

A dedicated low x trigger was used during data taking in 1995 and 1996. In addition to a scattered muon it required a hadron detected in the large calorimeter H2 [10], situated downstream of the spectrometer magnet (see Fig.1). The low x trigger,

$$\text{Trigger} = \text{H1H} \times \text{H2had} \times (\text{H3V} \cup \text{H3C}) \times \overline{\Sigma\text{VETO}} \tag{5}$$

was defined by the coincidence of signals from the scintillator hodoscope H1H, the hadronic part of the calorimeter H2had, the scintillator hodoscopes H3V or H3C and the anti-coincidence with ΣVETO. The coincidence H1H × H2had selected the charged hadrons, a hit in either one of H3V or H3C selected scattered muons and the anti-coincidence with ΣVETO prevented signals from halo muons already detected upstream of the target. The calorimeter H2, extending from 8.7 to 10.2 m from the magnet, had a beam hole of 20 cm diameter, while the hodoscope H3C was located at 13 m from the magnet and had a beam hole of 23 cm.

The threshold for the calorimeter signal was on average ten times the pulse–height for muons. Nevertheless, some contamination of the trigger by events without hadrons was observed. This was presumably due to electron showers produced by the beam scraping the sides of the calorimeter or the absorber hole. The rate of the low x triggers was about 500 events per beam spill of $4.5 \cdot 10^7$ muons. They were prescaled by a factor of eight for the deuteron run and a factor of four for the proton run. Very small muon scattering angles, including zero, were accepted for large energy transfers, $\nu > 110$ GeV, because the outgoing muons were deflected from the beam by the spectrometer magnet ($\int B\mathrm{d}l = 4.4$ Tm) and subsequently detected in H3V or H3C. This allowed the registration of events with values of x as low as 10^{-5}, extending the range of the standard triggers used in our previous analyses [4]. Those standard triggers were based exclusively on the detection of scattered muons and optimized for events with $x > 10^{-3}$ to avoid background from μe scattering.

The kinematic ranges in x and Q^2 covered by the low x trigger data and those from the standard triggers [4] are shown in Fig. 2. For the new data most events have $x < 0.01$. As for all the fixed target experiments the data at low values of x also have low values of Q^2.

4 Event selection

For the event selection, in addition to the criteria on the scattered muon (discussed later), the presence of additional particles with reconstructed tracks was required. For at least one such particle per event a minimum of 20% of its energy was required to have been deposited in the hadronic part of the calorimeter and this deposit was demanded to be larger than 1 GeV. This eliminated most of the electrons from the sample. The tracks had to be associated with the primary interaction vertex or with a secondary vertex formed by the decay products of neutral hadrons.

The x distributions for all events from the low x trigger and for the subsample with at least one track fulfilling the above criteria are compared in Fig. 3a. The peak at $x_{\mu\mathrm{e}} = m_\mathrm{e}/M_\mathrm{p} = 5.45 \cdot 10^{-4}$ corresponds to elastic scatters of muons off atomic electrons. This contamination was reduced by the event selection described above. To reduce it further an additional cut was applied to the class of events with exactly two tracks, a muon and a negatively charged particle. Fig. 3b shows the ratio of the particle momentum p to the momentum transfer $q = |\vec{p}_\mu - \vec{p}_\mu\,'|$ as a function of x for these events. Here $\vec{p}_\mu$ and $\vec{p}_\mu\,'$ denote incident and scattered muon momenta. The cluster of events around $p/q = 1$ and

$x = x_{\mu e}$ corresponds to μe scatters and was removed by cuts consistent with μe reaction kinematics: $3.55 \cdot 10^{-4} < x < 8.90 \cdot 10^{-4}$ and $0.63 < p/q < 1.27$. The remaining admixture of μe events (cf. Fig. 3a), in particular those accompanied by a photon radiated by the electron, was estimated to be $(5 \pm 1)\%$.

The analysis is limited to the kinematic region $x > 6 \cdot 10^{-5}$ and $Q^2 > 0.01$ GeV^2. The remaining cuts, listed below, are the same as those in the analysis of Ref. [4]. The momentum of the scattered muon was restricted to $p_\mu{}' > 19$ GeV to avoid the contamination by muons from the decay of pions and kaons produced in the target. The cut on the energy transfer to the nucleon, $\nu > 15$ GeV, rejects events with poor kinematic resolution, while the cut $y = \nu/E < 0.9$ removes events which would require large radiative corrections. Cuts on the vertex position were used to select interactions from the target material. A few per cent of the data were discarded because of instabilities in the beam intensity, detector efficiencies, and low target polarization. Effectively the above cuts removed about 50% of the data. The final samples of the low x trigger events consisted of $\sim 4.5 \times 10^6$ events for polarized protons and $\sim 1.4 \times 10^6$ events for polarized deuterons. In the newly explored range $6 \cdot 10^{-5} < x < 8 \cdot 10^{-4}$ this amounts to 1.4×10^6 and 0.5×10^6 events for the proton and the deuteron, respectively.

5 Asymmetry determination

In order to determine $A_\parallel$ accurately, in particular when its values are small, the counting rate asymmetry $A_\parallel^{\mathrm{meas}}$ is evaluated by combining data sets taken before and after a reversal of the target polarization [5]. The measured asymmetry is related to the cross section asymmetry $A_\parallel$ by $A_\parallel^{\mathrm{meas}} = f P_{\mathrm{t}} P_\mu A_\parallel$. The determination of $A_\parallel$ thus requires knowledge of the incident muon and target nucleon polarizations, P_μ and P_{t}, respectively, and the dilution factor f which accounts for the fact that only a fraction of the target nucleons is polarizable.

The presence of hadrons in the final state of the interaction reduces the number of events which do not carry information on the internal structure of the nucleon. There are two classes of such events. The first class consists of events from elastic scattering of muons off atomic electrons. The second class contains radiative events in which (quasi-)elastic scattering on target nuclei is accompanied by the radiation of a hard photon. These radiative events dilute the asymmetry similarly to the interactions on non-polarizable target nuclei. The effective dilution factor f'

$$f' = \frac{\sigma_{1\gamma}^{\mathrm{p,d}}}{\sigma^{\mathrm{p,d}}} f \quad = \frac{n_{\mathrm{p,d}} \sigma_{1\gamma}^{\mathrm{p,d}}}{\sum_{\mathrm{A}} n_{\mathrm{A}} \sigma^{\mathrm{A}}} \tag{6}$$

accounts for these diluting sources. The sum runs over all target nuclei including protons or deuterons; $n_{\mathrm{p,d,A}}$ are the numbers of nuclei of a given type in the target; $\sigma_{1\gamma}^{\mathrm{p,d}}$ are the one-photon-exchange (Born) cross sections and $\sigma^{p,d,A}$ are the sums of cross sections for all processes contributing to the selected sample of events. The sum in the denominator is smaller for muon scattering with hadron production than for the inclusive muon scattering. Therefore the effective dilution factor for events with hadrons is larger than for the inclusive sample, in particular at low x, as can be seen in Fig. 4. To obtain f' the cross sections were taken from the measurements of the structure function ratios of Ref. [11, 12] and the calculations of Ref. [13, 14]. In addition, for the bin $5 \cdot 10^{-4} < x < 8 \cdot 10^{-4}$, the effective dilution factor is reduced by 5% to account for the admixture of the $\mu - e$ elastic scatterings.

The finite resolution in the vertex position affects the separation of events originating from oppositely polarized target cells and results in more dilution. The vertex resolution depends on the scattering angle, thus on x, and is improved by the use of additional tracks for the vertex determination. This improvement is particularly important at low x. If only muon tracks were used to determine the vertex position for very small scattering angles (going down to zero), the uncertainty on the position would be very large, as can be seen in Fig. 5. Due to the improved vertex resolution given by the hadrons, the separation of the two target cells becomes possible even for the smallest scattering angles. The probability of an incorrect assignment, for example the association of the vertex to the wrong target cell, was estimated in bins of x by a simulation [15]. The resulting reduction of the effective dilution factor, the vertex smearing correction, ranges from about 2% in the highest to 15% in the lowest x bin.

Virtual photon asymmetries $A_1^{\mathrm{p,d}}$ for the proton and the deuteron were determined from $A_{\parallel}^{\mathrm{p,d}}$, according to Eq. (3) and subsequently corrected for the radiative background [13]. Since the presence of a hadron in the final state was required, only contributions from inelastic processes were retained in the calculation, as for the cross sections σ in Eq. (6).

To obtain the asymmetries A_1 information about unpolarized structure functions is required. The dependence of A_1 on $R = \sigma_{\mathrm{L}}/\sigma_{\mathrm{T}}$ enters through the depolarization factor D and through the radiative corrections. For $x > 0.003$ we used the same parametrization of R as in our previous analysis [4]. For $x < 0.003$ and $Q^2 < 1$ GeV^2, where R has not been measured, we used the parametrizations of σ_{L} and σ_{T} [16] obtained from a fit to the low Q^2 total electron–proton cross section measured at HERA. In the calculation of radiative corrections, in addition to R, the structure function F_2 down to Q^2 =0 is also needed. For $Q^2 > 0.2$ GeV^2 we used the same parametrization of F_2 as in Ref. [4] and below that value the model of Ref. [17].

It was shown in Ref. [4] that the inclusive asymmetry A_1 can be obtained from the sample of events with hadrons if the energy available for the hadronization, W, is large enough. Indeed the bias on the asymmetry, due to the loss of inelastic events by the limited acceptance of the spectrometer, was estimated to be smaller than 0.001 for a sample with $W > 12$ GeV. In the sample analyzed here W is comparable and in particular for $x < 0.002$ it is larger than 15 GeV. For this reason we expect that losses are of the same order as in Ref. [4], i.e. a few per cent, and that the bias on the asymmetry A_1 introduced by the hadron requirement can be neglected.

6 Systematic uncertainties on A_1

In our experiment asymmetries are obtained by combining the data taken before and after the reversal of the spin orientation in the two target cells [5]. This method leads to a significant reduction of the systematic uncertainties since the muon flux and the spectrometer acceptance need not be known, provided that the ratio of acceptances for events from the two target cells is the same before and after polarization reversal.

A potentially significant contribution to the systematic error is due to false asymmetries generated by instabilities of this acceptance ratio. The time dependence of the efficiencies of different parts of the detector was studied both for the scattered muon and the produced hadrons according to the method described in Ref. [5].

Another possibly important contribution to the systematic error on A_1 for $x < 0.003$ is due to the uncertainty on the function R. To estimate this contribution the lower limit $R = 0$ and the upper limit $R = 0.5$, consistent with results of the H1 measurements [18]

at low x and Q^2 about 10 GeV^2, were used. For $x > 0.003$ the uncertainty on R was calculated as in Ref. [4]. The effects due to uncertainties on R and F_2 in the computation of the radiative corrections were found to be negligible.

To evaluate the systematic uncertainty in the effective dilution factor f' we considered the contributions from the following sources: the uncertainty on the target composition, the limited precision of the measurements of the structure function ratios $F_2^{\rm A}/F_2^{\rm d}$ [11], $F_2^{\rm d}/F_2^{\rm p}$ [12] and of their extrapolations to the low x region, the precision of the cross sections in Eq. (6), the uncertainty on the contamination by μe events, and on the vertex smearing correction. As an estimate of the precision of $\sigma_{1\gamma}^{\rm p,d}/\sigma^{\rm p,d}$ in Eq. (6) we took the difference between results obtained with two calculations [13] and [14]. Its maximum value is about 5% in the lowest x bin and below 1% for $x > 8 \cdot 10^{-4}$. The contribution to $\sigma^{p,d}$ from inelastic scattering with hard photon emission was reduced due to the effective momentum cut in the acceptance for hadrons. A 30% uncertainty was then assigned to this contribution, leading to an additional few per cent uncertainty on the ratio $\sigma_{1\gamma}^{\rm p,d}/\sigma^{\rm p,d}$.

Other contributions to the systematic uncertainties, non-negligible at higher x, are the same as in Refs [4, 5]. The individual contributions to the systematic errors on $A_1^{\rm p,d}$ are presented in Table 1 for the proton and in Table 2 for the deuteron.

7 Results

The values of the asymmetries $A_1^{\rm p,d}$ are given in Tables 3 and 4 as functions of x at the average Q^2 in each bin. The total systematic error on A_1 has been obtained by combining in quadrature the individual contributions described in Sec. 6. In the last column of the tables the percentage of the low x triggers, simultaneously satisfying at least one of the standard triggers, is given. The overlap increases with increasing x, thus the new data give the new information mainly in low x and low Q^2 region.

The results on $A_1^{\rm p,d}$ are presented in Fig. 6. For $x < 8 \cdot 10^{-4}$ these are the first measurements of the spin asymmetries and are found consistent with zero within errors. For larger values of x the asymmetries from our previous measurements with standard triggers [4] are also shown. In Ref. [4], for $x < 0.02$, the presence of a hadron in the final state was required on the off-line level. Taking into account correlations, the two data sets are consistent in the kinematic region of overlap ($\chi^2/ndf = 12.6/11$ and $5.5/11$ for the proton and deuteron data, respectively).

The spin structure functions g_1 were calculated only for $x < 0.003$ and $Q^2 < 1$ GeV^2. from the results on the asymmetries A_1 using the relation $g_1 = A_1 \cdot F_2/[2x(1+R)]$. Here the same values of R as used in Sec. 5 have to be taken to be consistent with the A_1 determination, see Eq. (3, 4). The structure function F_2 was taken from the model of Ref. [17]. The values for g_1 are given in Tables 5 and 6 with the systematic errors resulting from propagation of the error on R and of the other individual contributions to systematic uncertainties on A_1. No uncertainty was associated with F_2. The results for $xg_1^{\rm p,d}$ are presented in Fig. 7 together with those from Ref. [4]. No significant spin effects are observed in the newly accessed kinematic region.

At small x, our data cover only very narrow intervals of x (or W) for fixed values of Q^2, cf. Fig. 2. Therefore they cannot be compared directly, without additional assumptions about the Q^2 dependence of g_1, with the Regge model which predicts small x behaviour of g_1 at fixed Q^2. However, these data can be compared with models predicting both the x and Q^2 dependence at low values of x and Q^2, see [19].

8 Conclusions

We have presented measurements of the longitudinal spin asymmetry A_1 for the proton and for the deuteron based on a dedicated low x trigger involving a hadron requirement. This method strongly reduces the background at low x and provides the possibility to investigate for the first time the range $6 \cdot 10^{-5} < x < 8 \cdot 10^{-4}$, $0.01 < Q^2 < 0.2$ GeV^2.

We do not observe any significant spin effects in this kinematic region while at larger x the measured asymmetries are in good agreement with our results in Ref. [4].

References

[1] See e.g. A. M. Cooper-Sarkar, R. C. E. Devenish and A. De Roeck, Int. J. Mod. Phys. **A13** (1998) 3385, and references therein.

[2] ZEUS Collaboration, J. Breitweg *et al.*, Phys. Lett. **B407** (1997) 432 and Eur. Phys. J. **C7** (1999) 609;
H1 Collaboration, C. Adloff *et al.* Nucl. Phys. **B497** (1997) 3.
See also T. Doyle, plenary talk at the XXIX Int. Conf. on High Energy Physics, Vancouver, Canada, July 1998.

[3] See e.g. A. Quadt, talk at the XXIX Int. Conf. on High Energy Physics, Vancouver, Canada, July 1998.

[4] SMC, B. Adeva *et al.*, Phys. Rev. **D58** (1998) 112001.

[5] SMC, D. Adams *et al.*, Phys. Rev. **D56** (1997) 5330.

[6] SMC, D. Adams *et al.*, Phys. Lett. **B336** (1994) 125;
E143, K. Abe *et al.*, Phys. Rev. **D58** (1998) 112003.

[7] N. Doble *et al.*, Nucl. Instr. Meth. **A343** (1994) 351.

[8] SMC, B. Adeva *et al.*, *The polarized double cell target of the SMC*, CERN-EP/99-31 and submitted to Nucl. Instr. Meth. A.

[9] SMC, B. Adeva *et al.*, Nucl. Instr. Meth. **A343** (1994) 363;
SMC, B. Adeva *et al.*, *Measurement of the SMC muon beam polarization using the asymmetry in the elastic scattering off polarized electrons*, to be published in Nucl. Instr. Meth. A.

[10] EMC, O. Allkofer *et al.*, Nucl. Instr. Meth. **179** (1981) 445.

[11] NMC, P. Amaudruz *et al.*, Z. Phys. **C51** (1991) 387; *ibid.* **C53** (1992) 73; Nucl. Phys. **B441** (1995) 3; M. Arneodo *et al.*, Nucl. Phys. **B441** (1995) 12; *ibid.* **B481** (1996) 3.

[12] NMC, M. Arneodo *et al.*, Nucl. Phys. **B487** (1997) 3.

[13] T.V. Kukhto and N.M. Shumeiko, Nucl. Phys. **B219** (1983) 412; I.V. Akushevich and N.M. Shumeiko, J. Phys. **G20** (1994) 513.

[14] A.A. Akhundov *et al.*, Fortsch. Phys. **44** (1996) 373.

[15] A. Steinmetz, Ph.D. Thesis, University of Mainz (1996).

[16] B. Surrow, Ph.D. Thesis, University of Hamburg (1998).

[17] B. Badełek and J. Kwieciński, Phys. Lett. **B295** (1992) 263.

[18] H1 Collaboration, C. Adloff *et al.*, Phys. Lett. **B393** (1997) 452; M. Klein, talk at the XXIX Int. Conf. on High Energy Physics, Vancouver, Canada, July 1998.

[19] B. Badełek and J. Kwieciński, hep-ph/9812297 to appear in J. Phys. **G25** (1999)

Table 1: Contributions to the systematic error on $A_1^{\rm p}(x)$ from the uncertainties on: the false asymmetry, $\Delta A_{\rm false}$; the target and the beam polarizations, $\Delta P_{\rm t}$ and ΔP_μ; the effective dilution factor, $\Delta f'$; the radiative corrections, Δrc; the neglect of A_2, ΔA_2; the ratio R, ΔR; and the background from polarized ^{14}N in the ammonia target, $\Delta P_{\rm bg}$.

$\langle x \rangle$	$\Delta A_{\rm false}$	$\Delta P_{\rm t}$	ΔP_μ	$\Delta f'$	Δrc	ΔA_2	ΔR	$\Delta P_{\rm bg}$
0.00010	0.0009	0.0005	0.0004	0.0014	0.0008	0.0000	0.0076	0.0009
0.00022	0.0011	0.0004	0.0003	0.0011	0.0006	0.0001	0.0045	0.0009
0.00039	0.0013	0.0001	0.0000	0.0001	0.0006	0.0001	0.0005	0.0009
0.00063	0.0014	0.0001	0.0001	0.0002	0.0006	0.0002	0.0009	0.0009
0.0010	0.0014	0.0006	0.0005	0.0008	0.0007	0.0003	0.0048	0.0009
0.0016	0.0014	0.0014	0.0011	0.0014	0.0007	0.0005	0.0096	0.0008
0.0025	0.0015	0.0005	0.0004	0.0006	0.0007	0.0008	0.0036	0.0008
0.0043	0.0018	0.0002	0.0002	0.0002	0.0008	0.0008	0.0003	0.0007
0.0078	0.0018	0.0009	0.0007	0.0006	0.0008	0.0010	0.0011	0.0006
0.0143	0.0019	0.0027	0.0021	0.0018	0.0007	0.0012	0.0033	0.0006
0.0245	0.0020	0.0022	0.0017	0.0015	0.0007	0.0003	0.0043	0.0005
0.0346	0.0020	0.0032	0.0025	0.0022	0.0007	0.0003	0.0050	0.0004
0.0487	0.0020	0.0009	0.0007	0.0006	0.0008	0.0004	0.0013	0.0004
0.077	0.0020	0.0074	0.0058	0.0048	0.0009	0.0004	0.0114	0.0006
0.121	0.0020	0.0104	0.0081	0.0068	0.0010	0.0004	0.0129	0.0009

Table 2: Contributions to the systematic error on $A_1^{\rm d}(x)$, with the same explanations as for Table 1, except that $\Delta P_{\rm bg}$ now refers to the contribution from protons in the deuterated butanol target.

$\langle x \rangle$	$\Delta A_{\rm false}$	$\Delta P_{\rm t}$	ΔP_μ	$\Delta f'$	Δrc	ΔA_2	ΔR	$\Delta P_{\rm bg}$
0.00010	0.0028	0.0001	0.0002	0.0007	0.0009	0.0000	0.0033	0.0002
0.00022	0.0034	0.0010	0.0011	0.0035	0.0007	0.0001	0.0146	0.0002
0.00039	0.0038	0.0005	0.0006	0.0015	0.0007	0.0001	0.0069	0.0002
0.00063	0.0041	0.0009	0.0010	0.0023	0.0007	0.0002	0.0103	0.0002
0.0010	0.0041	0.0006	0.0007	0.0011	0.0008	0.0003	0.0069	0.0002
0.0016	0.0043	0.0011	0.0013	0.0015	0.0008	0.0005	0.0113	0.0002
0.0025	0.0045	0.0002	0.0003	0.0003	0.0008	0.0008	0.0024	0.0002
0.0043	0.0052	0.0002	0.0002	0.0002	0.0009	0.0007	0.0004	0.0002
0.0078	0.0055	0.0008	0.0009	0.0008	0.0009	0.0008	0.0015	0.0002
0.0143	0.0057	0.0020	0.0023	0.0020	0.0009	0.0010	0.0035	0.0002
0.0245	0.0060	0.0002	0.0002	0.0002	0.0009	0.0015	0.0005	0.0002
0.0346	0.0061	0.0003	0.0003	0.0003	0.0009	0.0015	0.0006	0.0003
0.0487	0.0062	0.0012	0.0014	0.0012	0.0010	0.0016	0.0025	0.0004
0.077	0.0063	0.0014	0.0017	0.0013	0.0012	0.0004	0.0033	0.0006
0.121	0.0062	0.0000	0.0001	0.0000	0.0014	0.0004	0.0000	0.0008

Table 3: The asymmetry $A_1^{\rm p}(x)$ for the low x trigger data at the average Q^2 of each x-bin. The first error is statistical and the second is systematic. The first four bins are in the newly accessed kinematic region, while the remaining ones overlap with the standard triggers. The percentage of events overlapping with the standard triggers is given in the last column.

x Range	$\langle x \rangle$	$\langle Q^2 \rangle$ (GeV^2)	$A_1^{\rm p}$	%
0.00006–0.00015	0.00010	0.02	$0.016 \pm 0.016 \pm 0.008$	0
0.00015–0.00030	0.00022	0.06	$0.015 \pm 0.015 \pm 0.005$	0
0.0003 –0.0005	0.00039	0.10	$0.002 \pm 0.018 \pm 0.002$	0
0.0005 –0.0008	0.00063	0.17	$-0.004 \pm 0.020 \pm 0.002$	0
0.0008–0.0012	0.0010	0.26	$0.021 \pm 0.023 \pm 0.005$	12
0.0012–0.0020	0.0016	0.40	$0.045 \pm 0.022 \pm 0.010$	21
0.002–0.003	0.0025	0.63	$0.018 \pm 0.026 \pm 0.004$	29
0.003–0.006	0.0043	1.09	$-0.007 \pm 0.024 \pm 0.002$	35
0.006–0.010	0.0078	1.85	$0.028 \pm 0.030 \pm 0.003$	34
0.010–0.020	0.0143	3.15	$0.090 \pm 0.027 \pm 0.006$	31
0.020–0.030	0.0245	5.10	$0.073 \pm 0.039 \pm 0.006$	32
0.030–0.040	0.0346	7.0	$0.107 \pm 0.052 \pm 0.007$	37
0.040–0.060	0.0487	9.7	$0.029 \pm 0.049 \pm 0.003$	46
0.060–0.100	0.077	14.8	$0.248 \pm 0.054 \pm 0.016$	61
0.100–0.150	0.121	23.1	$0.345 \pm 0.078 \pm 0.020$	77

Table 4: The asymmetry $A_1^{\rm d}(x)$ for the low x trigger data at the average Q^2 of each x-bin, with the same presentation as for Table 3.

x Range	$\langle x \rangle$	$\langle Q^2 \rangle$ (GeV^2)	$A_1^{\rm d}$	%
0.00006–0.00015	0.00010	0.02	$-0.007 \pm 0.034 \pm 0.004$	0
0.00015–0.00030	0.00022	0.06	$0.048 \pm 0.033 \pm 0.015$	0
0.0003 –0.0005	0.00039	0.10	$0.027 \pm 0.039 \pm 0.008$	0
0.0005 –0.0008	0.00063	0.17	$0.043 \pm 0.043 \pm 0.011$	0
0.0008–0.0012	0.0010	0.26	$0.030 \pm 0.048 \pm 0.008$	15
0.0012–0.0020	0.0016	0.40	$-0.054 \pm 0.045 \pm 0.012$	23
0.002–0.003	0.0025	0.63	$-0.012 \pm 0.054 \pm 0.005$	31
0.003–0.006	0.0043	1.09	$-0.010 \pm 0.051 \pm 0.005$	36
0.006–0.010	0.0078	1.85	$0.039 \pm 0.062 \pm 0.006$	34
0.010–0.020	0.0143	3.15	$-0.098 \pm 0.057 \pm 0.008$	32
0.020–0.030	0.0245	5.09	$0.010 \pm 0.081 \pm 0.006$	32
0.030–0.040	0.0346	7.0	$-0.013 \pm 0.107 \pm 0.006$	36
0.040–0.060	0.0487	9.6	$-0.059 \pm 0.102 \pm 0.007$	44
0.060–0.100	0.077	14.7	$0.070 \pm 0.113 \pm 0.008$	59
0.100–0.150	0.121	22.9	$-0.002 \pm 0.165 \pm 0.006$	75

Table 5: The spin dependent structure function $g_1^{\rm p}(x)$ for the low x trigger data at the average Q^2 of each x-bin for $Q^2 < 1$ GeV^2. The first error is statistical and the second is systematic, which deos not include the uncertainty on F_2. The value of F_2 taken from the model of Ref.[17] in listed in the last column.

$\langle x \rangle$	$\langle Q^2 \rangle$ (GeV^2)	$g_1^{\rm p}$	$F_2^{\rm p}$
0.00010	0.02	$2.2 \pm 2.2 \pm 0.3$	0.028
0.00022	0.06	$2.0 \pm 2.1 \pm 0.4$	0.059
0.00039	0.10	$0.2 \pm 2.3 \pm 0.2$	0.099
0.00063	0.17	$-0.4 \pm 2.2 \pm 0.2$	0.140
0.0010	0.26	$1.9 \pm 2.1 \pm 0.4$	0.184
0.0016	0.40	$3.2 \pm 1.5 \pm 0.6$	0.233
0.0025	0.63	$0.9 \pm 1.4 \pm 0.2$	0.278

Table 6: The spin dependent structure function $g_1^{\rm d}(x)$ for the low x trigger data at the average Q^2 of each x-bin for $Q^2 < 1$ GeV^2 with the same presentation as for Table 5.

$\langle x \rangle$	$\langle Q^2 \rangle$ (GeV^2)	$g_1^{\rm d}$	$F_2^{\rm d}$
0.00010	0.02	$-1.0 \pm 4.7 \pm 0.4$	0.028
0.00022	0.06	$6.4 \pm 4.3 \pm 1.4$	0.059
0.00039	0.10	$3.3 \pm 4.8 \pm 0.9$	0.098
0.00063	0.17	$4.7 \pm 4.6 \pm 1.1$	0.140
0.0010	0.26	$2.7 \pm 4.3 \pm 0.7$	0.183
0.0016	0.40	$-3.8 \pm 3.2 \pm 0.8$	0.232
0.0025	0.63	$-0.6 \pm 2.8 \pm 0.3$	0.276

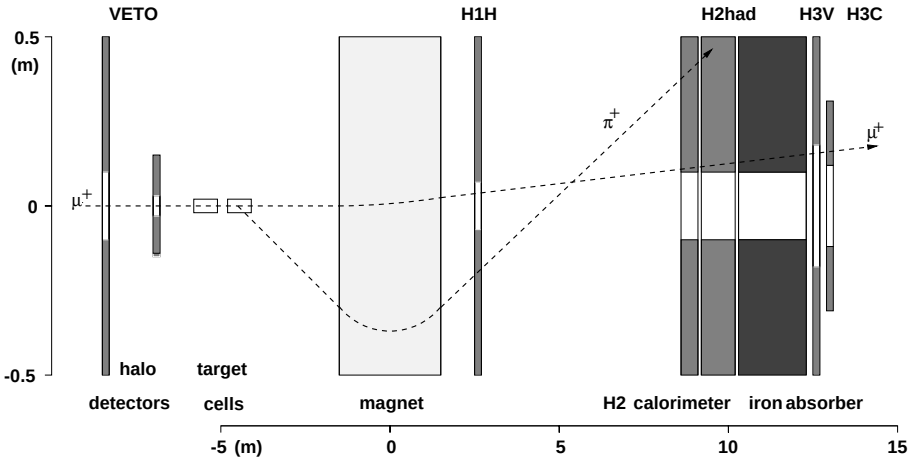

Figure 1: The detectors used for the definition of the low x trigger: the view is in the bending plane of the magnet. The detector planes and the beam holes within ± 0.5 m from the μ^+-beam axis are indicated . The vertical scale is expanded by factor of ten with respect to the horizontal one.

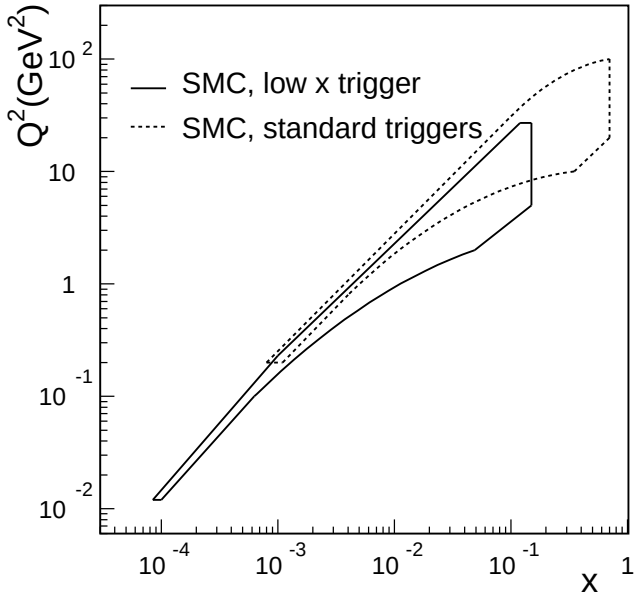

Figure 2: Contours of the kinematic acceptance in the (x, Q^2) plane for the standard triggers (dotted line) and for the low x trigger (continuous line).

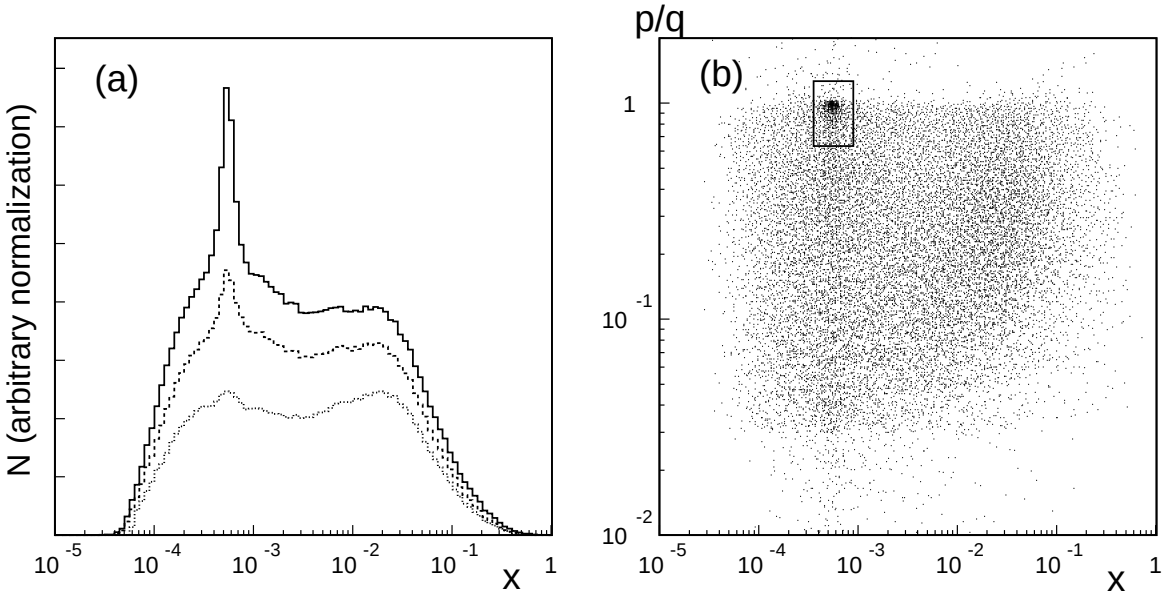

Figure 3: a) Event distributions as functions of x for the low x trigger without (continuous histogram) and with the requirement of a reconstructed hadron (dashed histogram) and after kinematic cuts discussed in the text (dotted histogram); b) the ratio of the particle momentum p to the momentum transfer $q = |\vec{p}_\mu - \vec{p}_\mu{}'|$ vs x for the low x trigger events with only one negative particle detected. Events within the box around $p/q = 1$ were removed from the sample.

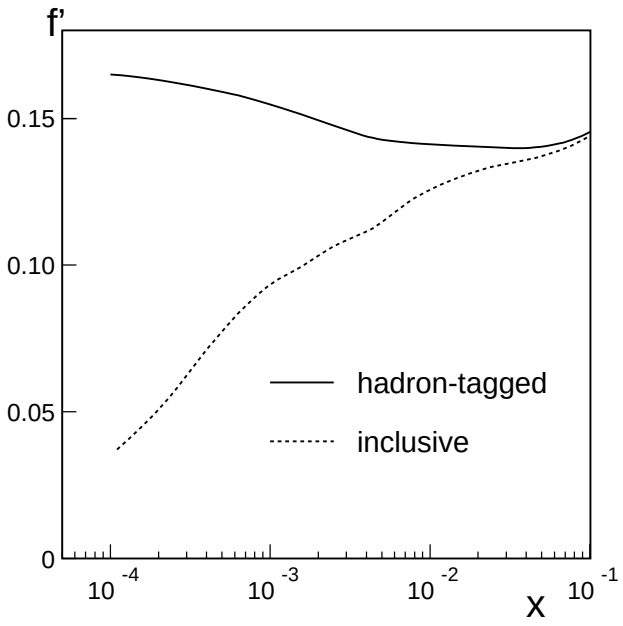

Figure 4: The effective dilution factor $f'(x)$ for the ammonia target for events with hadrons (continuous line) and for inclusive events (dotted line).

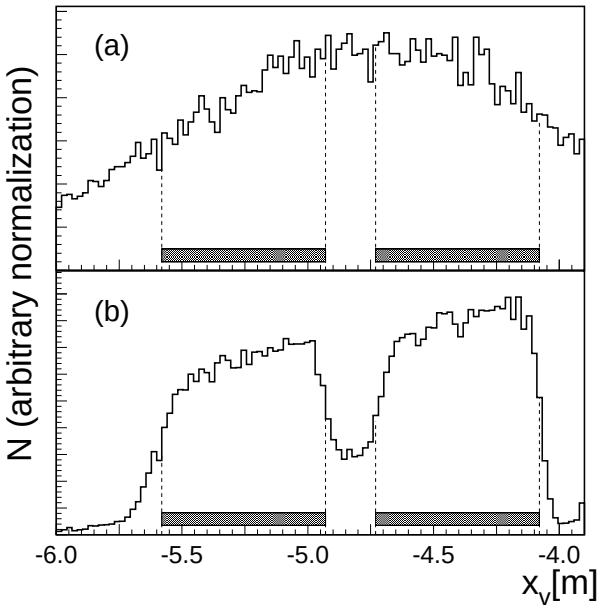

Figure 5: Distribution of the reconstructed vertex positions along the beam direction for events after kinematic cuts, in the lowest x interval ($6 \cdot 10^{-5} < x < 15 \cdot 10^{-5}$): a) distribution of vertices reconstructed using only incoming and outgoing muon tracks; b) distribution of vertices reconstructed using hadron tracks, too. The shaded boxes indicate the positions of the target cells. In between there is also a substantial contribution of events originating from the helium cooling liquid.

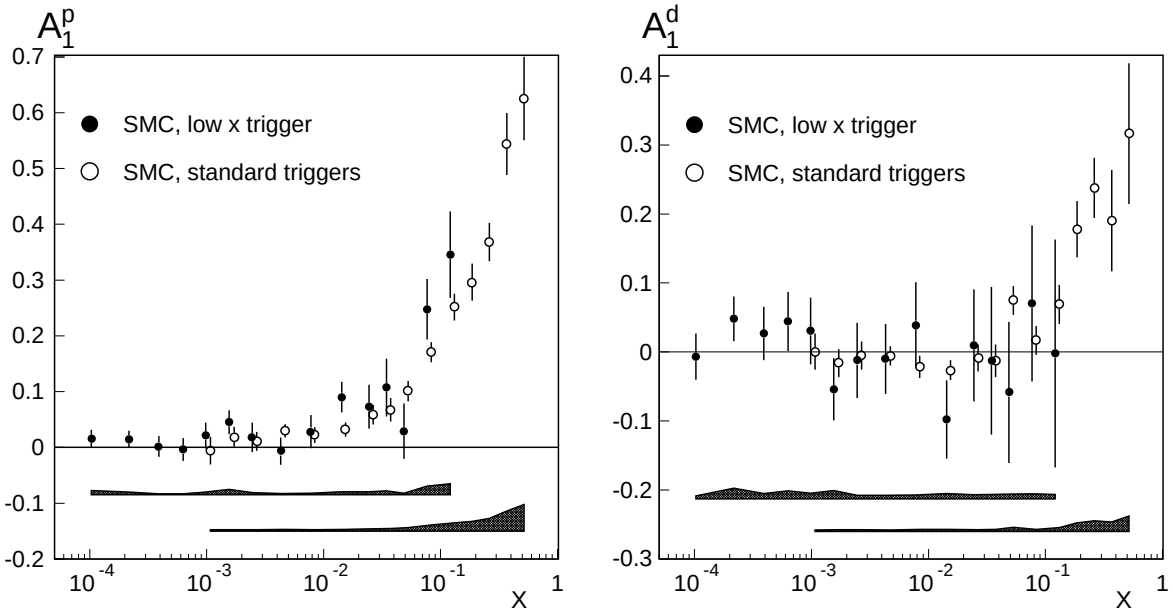

Figure 6: The asymmetry A_1 for the proton and for the deuteron as a function of x at the measured Q^2 obtained with the low x trigger (filled circles) together with those for standard triggers [4] (open circles). The shaded bands indicate the size of the respective systematic errors.

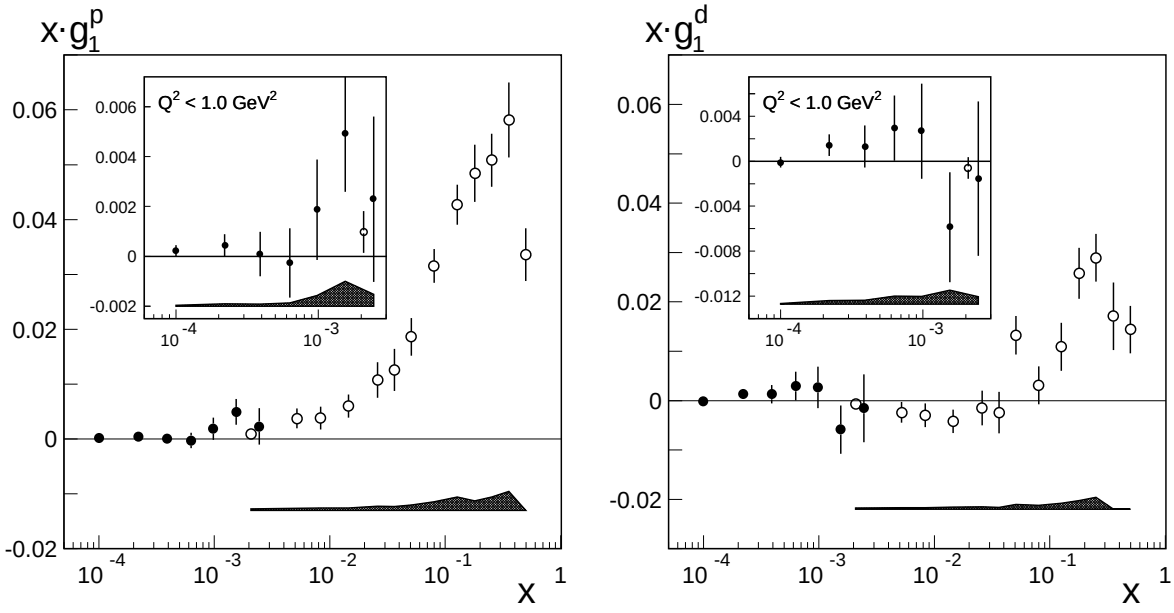

Figure 7: The values of xg_1 for the proton and for the deuteron as a function of x at the measured Q^2 obtained with the low x trigger (filled circles) together with those for standard triggers [4] (open circles). The low x trigger results are presented in the kinematic region where $Q^2 < 1$ GeV^2. The shaded bands indicate the size of the respective systematic errors.